

# Spin asymmetry for the elastic scattering of polarized electrons from Zn, Cd, and Hg

Mehrdad Adibzadeh<sup>1,\*</sup> and Constantine E. Theodosiou<sup>2,†</sup>

<sup>1</sup>*Department of Physics, University of West Florida, Pensacola, FL 32514, USA*

<sup>2</sup>*Department of Mathematics and Physics, Manhattan University, Riverdale, NY 10471, USA.*

(Dated: May 20, 2026)

We present an extensive set of theoretical results for spin asymmetry in the form of Sherman functions for the elastic scattering of electrons by zinc, cadmium, and mercury. This study extends the application of our earlier method of calculations, which we previously employed for stable inert gases and alkaline-earth-metals to these three atoms. Our predictions are in adequate agreement with experimental values and precise theoretical results.

PACS numbers: 34.80.Nz

## I. INTRODUCTION

The investigation of spin asymmetry in elastic electron scattering from atoms underscores the extent of spin-dependent interactions in electron-atom collisions. In the case of closed-shell atoms, which represent spin-zero targets, the spin asymmetry effects are due to the spin-orbit interactions. Thus the theoretical studies of spin asymmetry in elastic scattering from heavy closed shell atoms such as zinc, cadmium and mercury signifies the subtleties of relativistic effects and the antisymmetrization of the wave function.

Among the three atoms, mercury is the most studied through atomic collisions. Zinc and cadmium, although not as favorite as mercury, have been experimentally studied from the onset of the investigations into atomic collisions. The early studies, however, were all concentrated on cross sections. The studies into spin polarization effects followed later on and the interest in both experimental and theoretical approaches made an appearance.

For zinc, there is only one experimental work on the study of spin polarization of elastically scattered electrons, that of Bartsch et al. [1] for energies up to 14 eV. The theoretical investigations on the subject of spin polarization of elastically scattered electrons off zinc atom are those of McEachran and Stauffer [2], Kumar et al. [3], Szmytkowski and Sienkiewicz [4] and Bostock et al. [5].

In the case of cadmium, the only experimental work is that of Bartsch et al. [1] for energies up to 9 eV. The body of theoretical elastic spin asymmetry calculations on cadmium includes the works of Nahar [6], McEachran and Stauffer [2], Kumar et al. [3], Szmytkowski and Sienkiewicz [4], Berrington et al. [7] and Haque et al. [8].

Mercury, on the other hand, has enjoyed more attention from experiment and theory. There exist several spin polarization experimental investigations of elastically scattered electrons from mercury. They include works of Deichsel [9], Jost and Kessler [10], Deichsel et al. [11], Eitel et al. [12], Eitel and Kessler [13], Hanne et al. [14], Düweke et al. [15], Albert et al. [16], Hanne et al. [17], Berger et al. [18], Möllenkamp et al. [19], Berger and Kessler [20], Kaussen et al. [21] and Dümmler et al. [22]. The theoretical calculations of the subject include those of Bunyan [23], Bunyan and Schonfelder [24], Fink and Yates [25], Bartschat et al. [26], Haberland and Fritsche [27], McEachran and Stauffer [28], Sienkiewicz [29], Fritsche et al. [30], Szmytkowski and Sienkiewicz [4], Kelemen and Remeta [31], and Haque et al. [8, 32]

The present work intends to test our semi empirical approach (already applied to closed shell inert gas atoms and quasi-two-electron stable alkaline earth metal atoms [33–35]) for zinc, cadmium and mercury. In doing so, we will compare our results with only a reasonable number of dependable theoretical works, in addition to all available experimental data, in order to keep graphs readable.

## II. BRIEF REVIEW OF THE THEORETICAL AND COMPUTATIONAL APPROACH

In this work, we apply the same method of calculations as that described in our previous papers [33–35], i.e. the standard method of partial-wave expansion in potential scattering. We obtained the phase shifts by solving the

---

\*Electronic address: [madibzadeh@uwf.edu](mailto:madibzadeh@uwf.edu)

†Corresponding author: [constant.theodosiou@manhattan.edu](mailto:constant.theodosiou@manhattan.edu)

stationary Dirac equation, for which the choices of central static atomic, exchange, and polarization potentials were determined through an extensive analysis. The present choices for those potentials turned out to be the same as those of Refs. [34, 35].

To determine the combination for potentials, we performed an exhaustive analysis and comparison with the collection of all appropriate experimental and theoretical results on elastic electron scattering by inert gases and alkaline-earth metals. As a result we were able to recommend a combination of the central static atomic, exchange, and polarization potentials, which produced a consistent agreement between the calculated cross sections and reliable experimental and theoretical results at different projectile energies.

In the present work, we applied the same diligence to Zn, Cd and Hg to confirm our earlier choices for the only free parameter in our calculations: the cutoff radius of the polarization potential. Our analysis showed that the most consistent combination of potentials for Zn, Cd, and Hg was to be the Dirac-Slater atomic potential, the semi-classical exchange potential expression by Furness and McCarthy [36] and the Buckingham-type II polarization potential in the form

$$V_P(r) = -\frac{\alpha_d}{2(r^2 + r_c^2)^2}. \quad (1)$$

In the above equation,  $\alpha_d$  and  $r_c$  are the static atomic polarizability and the cutoff radius, respectively. The values for static polarizability,  $\alpha_d$ , were taken from the theoretical work of Kolb et al. [37].

Similar to our previous works, we required  $r_c$  to be a smooth, continuous and finite function of the scattered electron energy  $E$ . We further confirmed the functional behavior of this energy-dependent cutoff radius to be similar to those we used for alkaline-earth-metal atoms [34, 35] through comparisons with dependable theoretical and experimental data. Our careful analysis determined the value for the cutoff radius for zinc to be (in atomic units)

$$r_c(E) = \begin{cases} \frac{1}{3} \ln\left(\frac{E}{\mathcal{R}}\right) + \langle r \rangle_{4s} & E \geq 45\text{eV}, \\ 3.85 & E < 45\text{eV}, \end{cases} \quad (2)$$

for cadmium,

$$r_c(E) = \begin{cases} \frac{1}{3} \ln\left(\frac{E}{\mathcal{R}}\right) + \langle r \rangle_{5s} & E \geq 30\text{eV}, \\ 4.0 & E < 30\text{eV}, \end{cases} \quad (3)$$

and for mercury,

$$r_c(E) = \begin{cases} \frac{1}{3} \ln\left(\frac{E}{\mathcal{R}}\right) + \langle r \rangle_{6s} & E \geq 20\text{eV}, \\ 3.6 & E < 20\text{eV}. \end{cases} \quad (4)$$

Here  $E$  is the energy of the incident electron in eV,  $\mathcal{R}$  is the Rydberg constant ( $\mathcal{R} = 13.605\,691\,72$  eV), and  $\langle r \rangle_{4s} = 2.680 a_0$ ,  $\langle r \rangle_{5s} = 2.978 a_0$  and  $\langle r \rangle_{6s} = 3.045 a_0$  are the expectation values of zinc's 4s shell, cadmium's 5s shell, and mercury's 6s shell radii, respectively. The cutoff radii for low energies are set to constant values to avoid the logarithmic anomaly. The reader may find more details on this constant value and its behavior below an energy threshold in Ref. [34]. To determine the low energy constant values for  $r_c$ , we made numerous comparisons with accurate theoretical data for integrated cross section as guidance.

Once the Dirac Hamiltonian is determined and the Dirac equation is solved, we can obtain the spin-up  $\delta_l^+$  and spin-down  $\delta_l^-$  phase shifts, which are used to determine the direct,  $f$ , and spin-flip,  $g$ , scattering amplitudes

$$f(\theta, k) = \frac{1}{k} \sum_{l=0}^{\infty} \left[ (l+1) e^{i\delta_l^+(k)} \sin \delta_l^+(k) + l e^{i\delta_l^-(k)} \sin \delta_l^-(k) \right] P_l(\cos \theta), \quad (5)$$

and

$$g(\theta, k) = \frac{1}{k} \sum_{l=0}^{\infty} \left[ e^{i\delta_l^-(k)} \sin \delta_l^-(k) - e^{i\delta_l^+(k)} \sin \delta_l^+(k) \right] P_l^1(\cos \theta). \quad (6)$$

In the above equations,  $k$  and  $\theta$  are the wave number of the incident electron and the scattering angle, respectively. The Sherman function (SF), which describes the measured spin asymmetries in the number of scattered electrons is expressed in terms of scattering amplitudes as [38, 39]

$$S(\theta, k) = i \frac{f(\theta, k)g^*(\theta, k) - f^*(\theta, k)g(\theta, k)}{|f(\theta, k)|^2 + |g(\theta, k)|^2}. \quad (7)$$

Once again, we used our modified version of the Dirac-Slater code by Salvat et al. [40] in our calculations and throughout this work and for all considered energies, we used up to 150 partial-wave phase shifts.

### III. RESULTS AND DISCUSSION

Since we would like to compare our results with all available experimental measurements, to maintain graph readability, we will limit the comparisons to most recent and reliable data whenever possible. We also avoid the placement of error bars on experimental data if the uncertainty may be encompassed through an appropriate size of the marker.

#### A. Zinc

The experimental data on spin asymmetry for elastic electron scattering off zinc are limited to those of Bartcsh et al. [1] for a few energies between 2 eV and 14 eV. At impact energies for which experimental data are available, we compare our Sherman functions with the experiment and other theoretical results in figures 1 and 2. These comparisons include the relativistic distorted-wave (RDW) calculations of McEachran and Stauffer [2] and Szmytkowski and Sienkiewicz [4] and the 66-state relativistic convergent close coupling (RCCC) formulation of Bostock et al. [5]. In figure 3, we exclusively compare with the available RCCC calculations at 7 and 7.5 eV, for which no experimental data are available.

The present Sherman function values at 2 eV impact energy are in outstanding agreement with experiment, as seen in figure 1. This agreement is to a lesser extent on display at 3 eV as well. Nonetheless, the agreement of our Sherman functions at 4 and 5 eV with experiment is mostly limited to the forward direction, while the RCCC calculations present excellent agreement with experiment. For impact energies 6 and 9 eV, on figure 2, our Sherman functions again show excellent agreement with experiment and the RCCC results in the forward direction. This is while both RDW calculations at 9 eV indicate a considerable disagreement with experiment.

The most interesting comparisons, however, are those at 11 and 14 eV impact energies in figure 2. At 11 eV, our values show a better agreement with experiment than those of the RCCC calculations. As touched upon by Ref. [5], the discrepancy between the RCCC Sherman function and experiment at 11 eV, is due to  $3d^{10}$  excitations which were not modeled accurately by the RCCC formalism. Considering our single-channel method of calculations does not include the effects of excited states on elastic spin asymmetry, our agreement with experiment is quite interesting. At 14 eV, the present Sherman functions display a comparable agreement with experiment as that between RCCC and experiment. In figure 3, we compare our Sherman functions at 7 and 7.5 eV with those of the RCCC calculations with discrepancies to note. These slight differences are the positions of the maxima and the values of the minima of the Sherman function at the two energies, which were observed also at other impact energies.

Finally, a three-dimensional (3D) graph of present Sherman function versus impact energy and scattering angle for elastic  $e$ -Zn scattering is provided in figure 4 to obtain a comprehensive view of the behavior of  $S(\theta, E)$ .

#### B. Cadmium

The measurements of Bartcsh et al. [1] are the only experimental data on spin asymmetry for elastic electron scattering off cadmium. We compare our Sherman functions, in figures 5, 6 and 7, with all experimental data in conjunction with other theoretical works, which include the 55-state RCCC method and the relativistic optical potential (ROP) calculations of Berrington et al. [7] and the relativistic polarized orbital approach of Szmytkowski and Sienkiewicz [4]. Very good agreement with experiment is observed for energies up to 2 eV, in particular in the forward direction. The agreement at these energies with RCCC results is at least qualitative if not very good. For energies above 2 eV, in particular approaching the  $(5s5p) \ ^3P_{0,1,2}$  excited states, and the  $(5s5p^2) \ ^3D_{3/2,5/2}$  negative ion state, our agreement with experiment is rather spotty. Setting aside the accurate RCCC predictions, other single-channel calculations do not agree with experiment at these energies either.

Our Sherman functions at 5 and 6 eV impact energies, show an excellent agreement with experiment in the forward direction, while disagreeing by a few degrees on the location of the maximum with RCCC Sherman functions. At both energies, ROP results show considerable discrepancies with experiment. Our Sherman function at 9 eV displays a remarkable agreement with experiment while RCCC's is the only other calculation in agreement with experiment at this energy. In figure 8, we present our Sherman function values at  $110^\circ$  as a function of energy in comparison with the experiment and the theoretical results from the RCCC and ROP approaches. The swift rise in Sherman function values at  $110^\circ$  between 3.7 and 4.2 eV is due to the formation of negative ion resonances and excited states in this energy interval (discussed in Ref. [41]). Our Sherman function at  $110^\circ$ , shows a displaced ascend while following the experiment and RCCC through a downward bias. The overall energy-behavior of our results is good in spite of the single-channel nature of the approach.

The 3D graph of Sherman function against impact energy and scattering angle for elastic  $e$ -Cd scattering is presented in figure 9.

### C. Mercury

As mentioned in the introduction for mercury there is a plethora of spin asymmetry measurements, some of them going back to 1956. The work of Düweke et al. [15] is limited to energies below 4 eV and that of Dümmler et al. [22] to less than 2 eV. Above 6 eV impact energy, we have the works of Kaussen et al. [21] (6-24, and 180 eV), Hanne et al. [17] (8, 10, 12, and 18 eV), and Deichsel et al. [11] (3.5, 7, 23, and 45 eV). At intermediate energies, there exist the works of Eitel et al. [12] (18.3, 25, 30, 50, and 180 eV) and that of Berger and Kessler [20] (25, 35, 50, and 150 eV). Finally, at the upper range of impact energies we have the works of Jost and Kessler [10] (180 to 340 eV) and Eitel et al. [12] (100 - 2000 eV). Thus we have experimental data in a wide range of impact energies to compare our theoretical predictions with.

In Figures 10 – 20, we present a detailed comparison of our Sherman functions for mercury, from 1 eV through 500 eV, with experimental and select theoretical data. The theoretical works in the comparisons include the 66-state RCCC calculations of Bostock et al. [5], the R-matrix calculations of Bartschat et al. [26], the generalized density-functional calculations (GDF) of Haberland and Fritsche [27], the relativistic distorted wave method (RDW) of McEachran and Stauffer [28], and the optical potential (OP) calculations of Haque et al. [32].

In figure 10, our Sherman functions display a very good agreement with the measurements of Dümmler et al. [22] at energies 1, 1.5 and 1.9 eV. In the same figure and at energy 2.4 eV, the RCCC and our Sherman functions only exhibit partial agreement with the experimental data of Düweke et al. [15]. At energies 3.5, 3.9, 6 and 7 eV, present Sherman functions agree with experiment quite well but mainly in the forward direction, as shown in figure 11.

In figure 12, our values agree with the measurements of Hanne et al. [17] at impact energies 8 and 10 eV while throughout the angular range disagreeing with the OP predictions at those energies. In the same figure, our data show a considerably good agreement with the experiment of Kaussen et al. [21] and RCCC values at 9 and 11 eV.

We observe an excellent agreement, in figure 13, with experiment at 12 eV. Very good agreement with experiment is also on display at 12.2 and 14 eV, while not quite reaching the measured values at the two minima of  $S(\theta)$ . The agreement with experiment at 15 eV is better in the forward direction while notable disagreement is observed with the values of OP calculations.

Our Sherman functions, in figure 14, show good agreement with the experimental results of Kaussen et al. [21] at 17 and 24 eV. However, considerable disagreement is observed with the measurements of Hanne et al. [17] at 18 eV and Deichsel et al. [11] at 23 eV. There are no other theoretical data to compare with at these energies.

For energies above 23 eV it is clear that theory predicts accurately the experimentally confirmed physics of electron polarization during elastic scattering from mercury. In figure 15, present results display good agreement with experimental data while slightly disagreeing with those of OP on the positions of the first minimum and the maximum at 25 eV impact energy. The RDW results follow nicely our values.

Present Sherman functions, in figure 16, display excellent agreement with experimental data. Our values differ from those of RDW at 150 eV only in the backward direction whereas visible differences are on display between our Sherman functions and those of the OP calculations at 100, 170 and 180 eV in figure 16.

At higher impact energies, our results are in excellent agreement with the available experimental data as shown in figures 17– 19. No other calculations exist in this energy range, other than an OP one at 500 eV.

In figure 20, we compare our Sherman function values at  $50^\circ$  with measurements of Albert et al. [16], at  $60^\circ$  with those of Dümmler et al. [22], and at  $75^\circ$  and  $90^\circ$  with the experimental results of Hanne et al. [17], Jost and Kessler [10], Mölenkamp et al. [19] and Eitel and Kessler [13] for various energy intervals. Overall the agreement with experimental data is very good.

Further comparisons with experimental data of Mölenkamp et al. [19] and Eitel et al. [12] at  $90^\circ$  are displayed in figure 21 for energies up to 2600 eV exhibiting excellent agreement. In the same figure, our Sherman function values

at  $117^\circ$  and  $135^\circ$  show a strong disagreement in the energy interval of 4 - 6 eV with measurements of Düweke et al. [15] and Albert et al. [16], respectively. This is not very surprising as our Sherman functions did not display good agreements with experimental data in backward direction at those energies (see figure 11).

Finally, figure 22 displays the 3D graph of Sherman function against impact energy and scattering angle for elastic e-Hg scattering to provide a global perspective.

#### IV. CONCLUSIONS

In this work we extended our previous work using a self-consistent Dirac-Slater calculation of the spin polarization of elastically scattered electrons from Zn, Cd, and Hg. The central target potential was supplemented with a core-polarization term which contains the only adjustable parameter of this approach, i.e. the cut-off radius of the polarization potential. We view the overall agreement with all the available experimental data and sophisticated calculations quite satisfactory. The present comprehensive data aim to serve as a reliable reference point for future investigations.

- 
- [1] M. Bartsch, H. Geesmann, G. F. Hanne, and J. Kessler, *Journal of Physics B: Atomic, Molecular and Optical Physics* **25**, 1511 (1992), URL <https://dx.doi.org/10.1088/0953-4075/25/7/021>.
  - [2] R. P. McEachran and A. D. Stauffer, *Journal of Physics B: Atomic, Molecular and Optical Physics* **25**, 1527 (1992), URL <https://dx.doi.org/10.1088/0953-4075/25/7/022>.
  - [3] P. Kumar, A. K. Jain, A. N. Tripathi, and S. N. Nahar, *Phys. Rev. A* **49**, 899 (1994), URL <https://link.aps.org/doi/10.1103/PhysRevA.49.899>.
  - [4] R. Szmytkowski and J. E. Sienkiewicz, *Journal of Physics B: Atomic, Molecular and Optical Physics* **27**, 555 (1994), URL <https://dx.doi.org/10.1088/0953-4075/27/3/019>.
  - [5] C. J. Bostock, D. V. Fursa, and I. Bray, *Phys. Rev. A* **85**, 062707 (2012), URL <https://link.aps.org/doi/10.1103/PhysRevA.85.062707>.
  - [6] S. N. Nahar, *Phys. Rev. A* **43**, 2223 (1991), URL <https://link.aps.org/doi/10.1103/PhysRevA.43.2223>.
  - [7] M. J. Berrington, C. J. Bostock, D. V. Fursa, I. Bray, R. P. McEachran, and A. D. Stauffer, *Phys. Rev. A* **85**, 042708 (2012), URL <https://link.aps.org/doi/10.1103/PhysRevA.85.042708>.
  - [8] M. M. Haque, A. K. Haque, M. A. Uddin, M. Maaza, M. A. R. Patoary, A. K. Basak, and B. C. Saha (Academic Press, 2021), vol. 84 of *Advances in Quantum Chemistry*, pp. 1–72, URL <https://www.sciencedirect.com/science/article/pii/S0065327620300046>.
  - [9] H. Deichsel, *Zeitschrift für Physik* **164**, 156 (1961).
  - [10] K. Jost and J. Kessler, *Zeitschrift für Physik* **195**, 1 (1966).
  - [11] H. Deichsel, E. Reichert, and H. Steidl, *Zeitschrift für Physik* **189**, 212 (1966).
  - [12] W. Eitel, K. Jost, and J. Kessler, *Phys. Rev.* **159**, 47 (1967), URL <https://link.aps.org/doi/10.1103/PhysRev.159.47>.
  - [13] W. Eitel and J. Kessler, *Zeitschrift für Physik A Hadrons and nuclei* **241**, 355 (1971).
  - [14] G. Hanne, K. Jost, and J. Kessler, *Zeitschrift für Physik* **252**, 141 (1972).
  - [15] M. Düweke, N. Kirchner, E. Reichert, and S. Schön, *Journal of Physics B: Atomic and Molecular Physics* **9**, 1915 (1976), URL <https://dx.doi.org/10.1088/0022-3700/9/11/017>.
  - [16] K. Albert, C. Christian, T. Heindorff, E. Reichert, and S. Schön, *Journal of Physics B: Atomic and Molecular Physics* **10**, 3733 (1977), URL <https://doi.org/10.1088/0022-3700/10/18/029>.
  - [17] G. F. Hanne, K. J. Kollath, and W. Wubker, *Journal of Physics B: Atomic and Molecular Physics* **13**, L395 (1980), URL <https://dx.doi.org/10.1088/0022-3700/13/12/009>.
  - [18] O. Berger, J. Kessler, K. J. Kollath, R. Möllenkamp, and W. Wübker, *Phys. Rev. Lett.* **46**, 768 (1981), URL <https://link.aps.org/doi/10.1103/PhysRevLett.46.768>.
  - [19] R. Möllenkamp, W. Wübker, O. Berger, K. Jost, and J. Kessler, *Journal of Physics B: Atomic and Molecular Physics* **17**, 1107 (1984), URL <https://doi.org/10.1088/0022-3700/17/6/022>.
  - [20] O. Berger and J. Kessler, *Journal of Physics B: Atomic and Molecular Physics* **19**, 3539 (1986), URL <https://dx.doi.org/10.1088/0022-3700/19/21/018>.
  - [21] F. Kaussen, H. Geesmann, G. F. Hanne, and J. Kessler, *Journal of Physics B: Atomic and Molecular Physics* **20**, 151 (1987), URL <https://dx.doi.org/10.1088/0022-3700/20/1/018>.
  - [22] M. Dümmler, M. Bartsch, H. Geesmann, G. F. Hanne, and J. Kessler, *Journal of Physics B: Atomic, Molecular and Optical Physics* **25**, 4281 (1992), URL <https://dx.doi.org/10.1088/0953-4075/25/20/022>.
  - [23] P. J. Bunyan, *Proceedings of the Physical Society* **81**, 816 (1963), URL <https://doi.org/10.1088/0370-1328/81/5/304>.
  - [24] P. J. Bunyan and J. L. Schonfelder, *Proceedings of the Physical Society* **85**, 455 (1965), URL <https://doi.org/10.1088/0370-1328/85/3/306>.
  - [25] M. Fink and A. C. Yates, *Atomic Data and Nuclear Data Tables* **1**, 385 (1969), ISSN 0092-640X, URL <https://www.sciencedirect.com/science/article/pii/S0092640X6980029X>.

- [26] K. Bartschat, K. Blum, P. G. Burke, G. F. Hanne, and N. S. Scott, *Journal of Physics B: Atomic and Molecular Physics* **17**, 3797 (1984), URL <https://doi.org/10.1088/0022-3700/17/18/016>.
- [27] R. Haberland and L. Fritsche, *Journal of Physics B: Atomic and Molecular Physics* **20**, 121 (1987), URL <https://dx.doi.org/10.1088/0022-3700/20/1/016>.
- [28] R. P. McEachran and A. D. Stauffer, *Journal of Physics B: Atomic and Molecular Physics* **20**, 5517 (1987), URL <https://dx.doi.org/10.1088/0022-3700/20/20/027>.
- [29] J. E. Sienkiewicz, *Journal of Physics B: Atomic, Molecular and Optical Physics* **23**, 1869 (1990), URL <https://dx.doi.org/10.1088/0953-4075/23/11/020>.
- [30] L. Fritsche, C. Kroner, and T. Reinert, *Journal of Physics B: Atomic, Molecular and Optical Physics* **25**, 4287 (1992), URL <https://dx.doi.org/10.1088/0953-4075/25/20/023>.
- [31] V. I. Kelemen and E. Y. Remeta, *Journal of Physics B: Atomic, Molecular and Optical Physics* **45**, 185202 (2012), URL <https://dx.doi.org/10.1088/0953-4075/45/18/185202>.
- [32] A. K. F. Haque, M. M. Haque, P. P. Bhattacharjee, M. A. Uddin, M. A. R. Patoary, M. I. Hossain, A. K. Basak, M. S. Mahbub, M. Maaza, and B. C. Saha, *Journal of Physics Communications* **1**, 035014 (2017), URL <https://doi.org/10.1088/2399-6528/aa8bf8>.
- [33] M. Adibzadeh and C. E. Theodosiou, *Atomic Data and Nuclear Data Tables* **91**, 8 (2005), ISSN 0092-640X, URL <https://www.sciencedirect.com/science/article/pii/S0092640X05000343>.
- [34] M. Adibzadeh and C. E. Theodosiou, *Phys. Rev. A* **70**, 052704 (2004), URL <https://link.aps.org/doi/10.1103/PhysRevA.70.052704>.
- [35] M. Adibzadeh, C. E. Theodosiou, and N. J. Harmon, *Atoms* **12** (2024), ISSN 2218-2004, URL <https://www.mdpi.com/2218-2004/12/6/33>.
- [36] J. B. Furness and I. E. McCarthy, *Journal of Physics B: Atomic and Molecular Physics* **6**, 2280 (1973), URL <https://dx.doi.org/10.1088/0022-3700/6/11/021>.
- [37] D. Kolb, W. R. Johnson, and P. Shorer, *Phys. Rev. A* **26**, 19 (1982), URL <https://link.aps.org/doi/10.1103/PhysRevA.26.19>.
- [38] N. Sherman, *Phys. Rev.* **103**, 1601 (1956), URL <https://link.aps.org/doi/10.1103/PhysRev.103.1601>.
- [39] J. Kessler, *Rev. Mod. Phys.* **41**, 3 (1969), URL <https://link.aps.org/doi/10.1103/RevModPhys.41.3>.
- [40] F. Salvat, J. Fernández-Varea, and W. Williamson, *Computer Physics Communications* **90**, 151 (1995), ISSN 0010-4655, URL <https://www.sciencedirect.com/science/article/pii/0010465595000391>.
- [41] C. J. Bostock, M. J. Berrington, D. V. Fursa, and I. Bray, *Phys. Rev. Lett.* **107**, 093202 (2011), URL <https://link.aps.org/doi/10.1103/PhysRevLett.107.093202>.

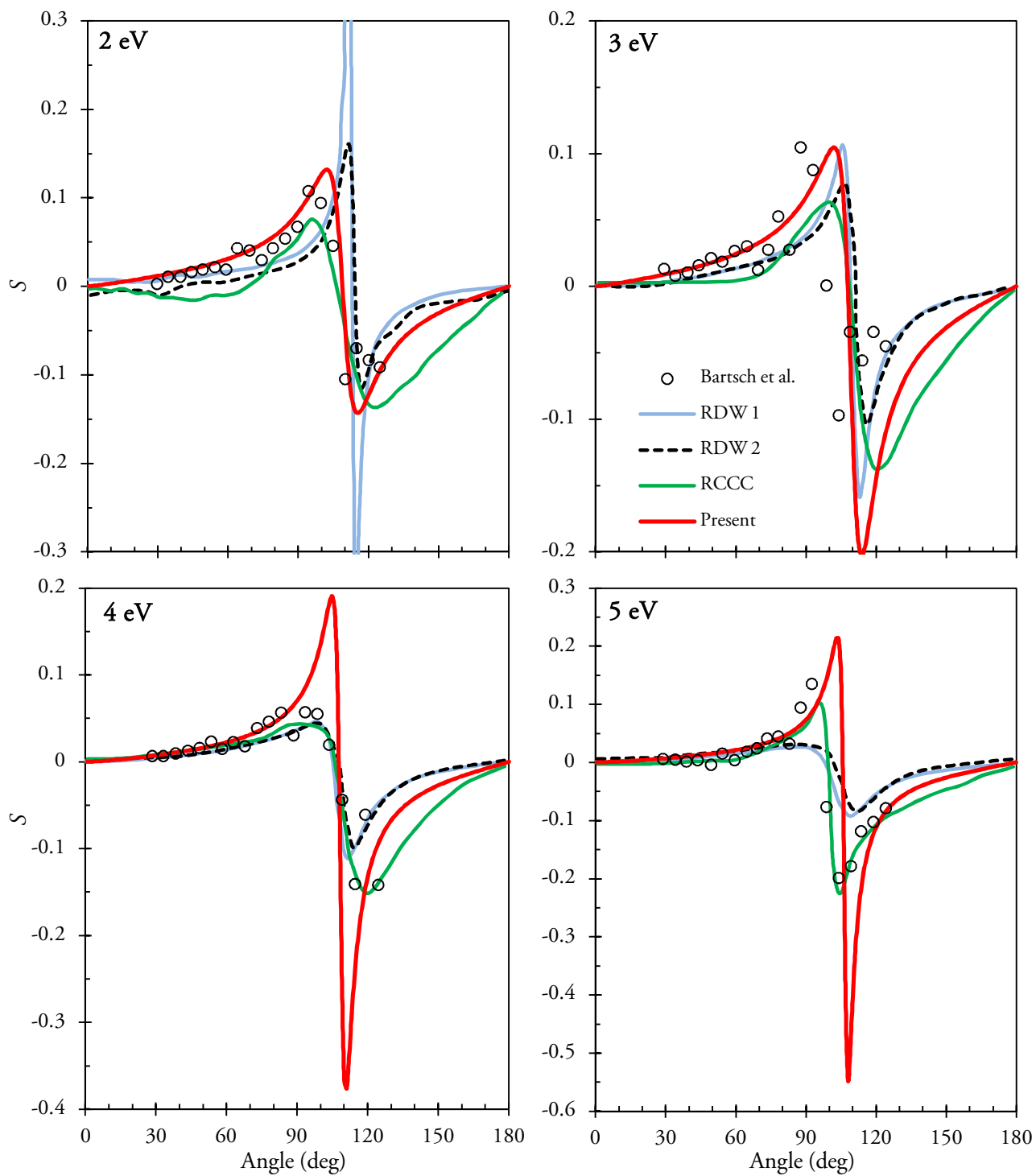


FIG. 1: Sherman function for electron scattering from zinc at 2, 3, 4 and 5 eV: The legend in the figure describes markers for Present work; Experiment: Bartsch et al. [1]; Other theoretical: 66-state RCCC [5], RDW 1 [2] and RDW 2 [4].

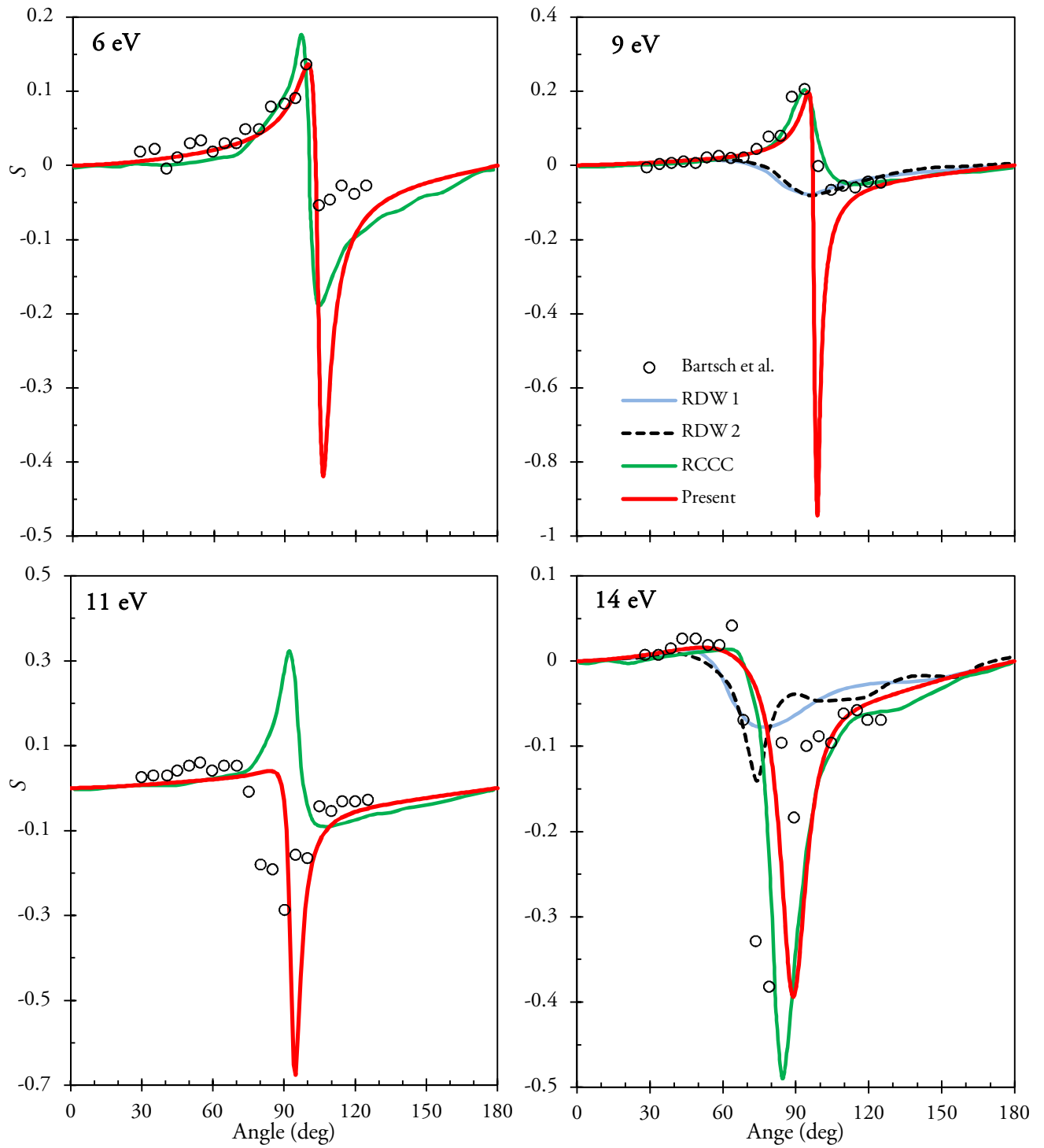


FIG. 2: Same as for figure 1 but at 6, 9, 11 and 14 eV projectile energies.

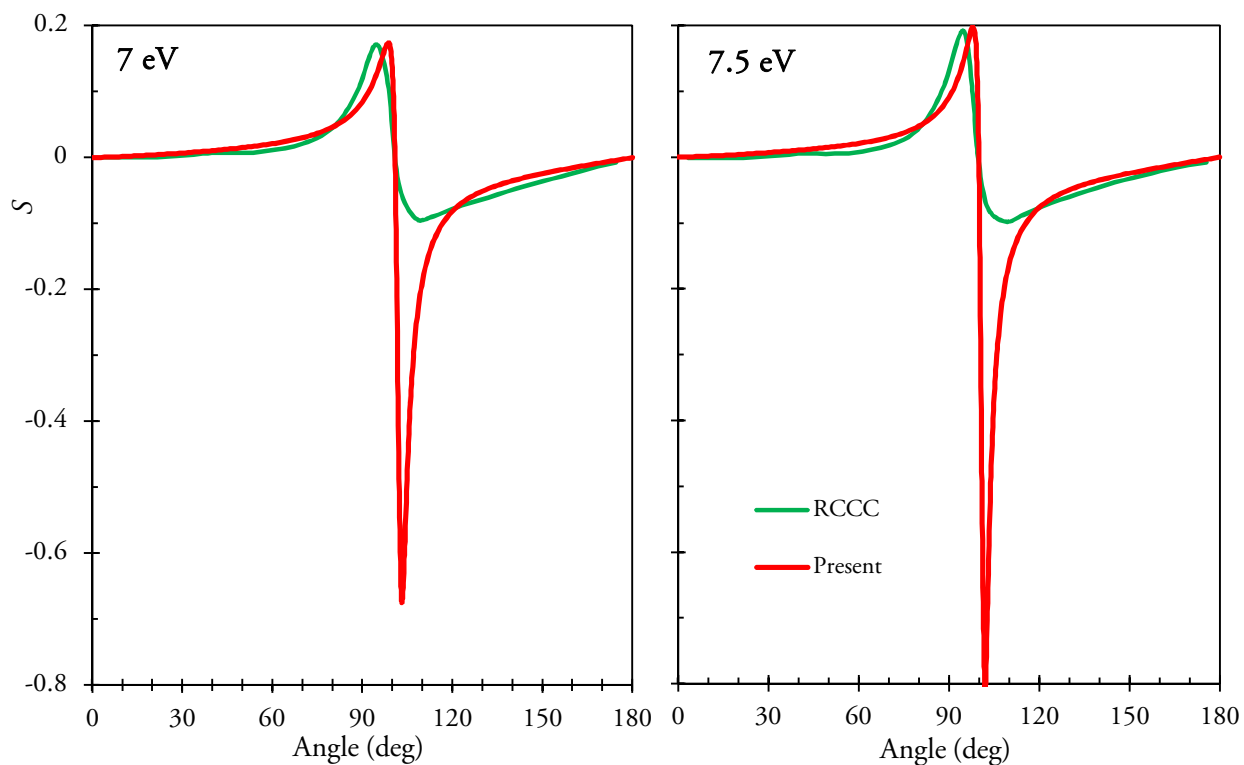


FIG. 3: Comparisons between present Sherman function values at 7 and 7.5 eV with those of 66-state RCCC [5] calculations.

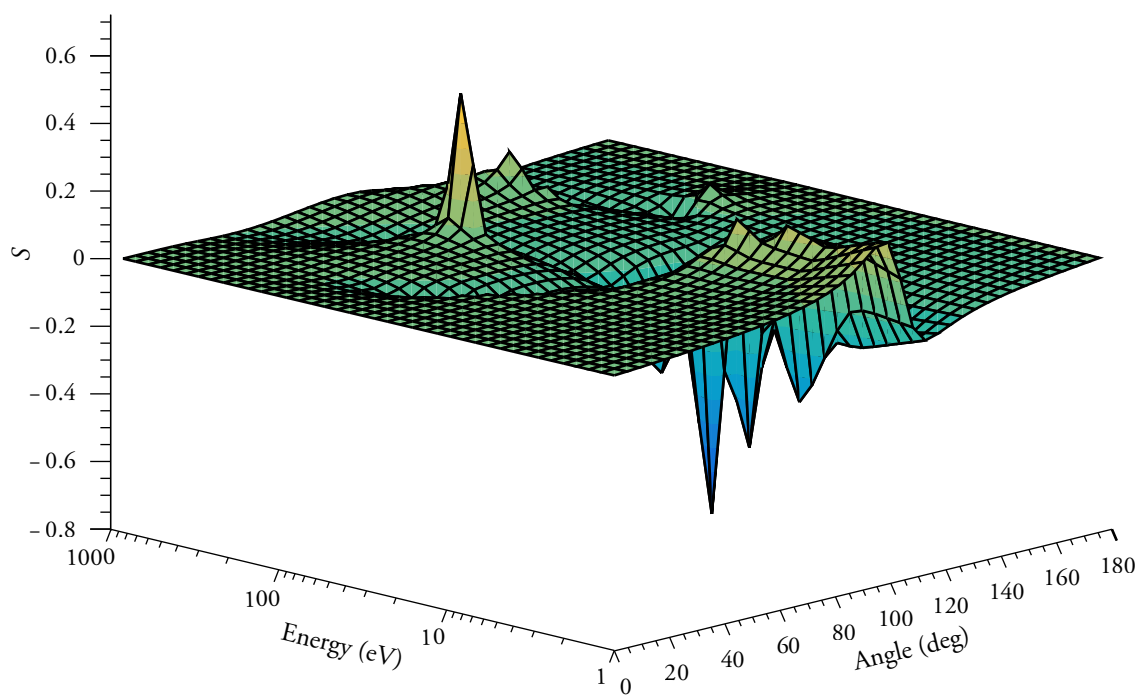


FIG. 4: A three-dimensional view of Sherman function for electron scattering from zinc.

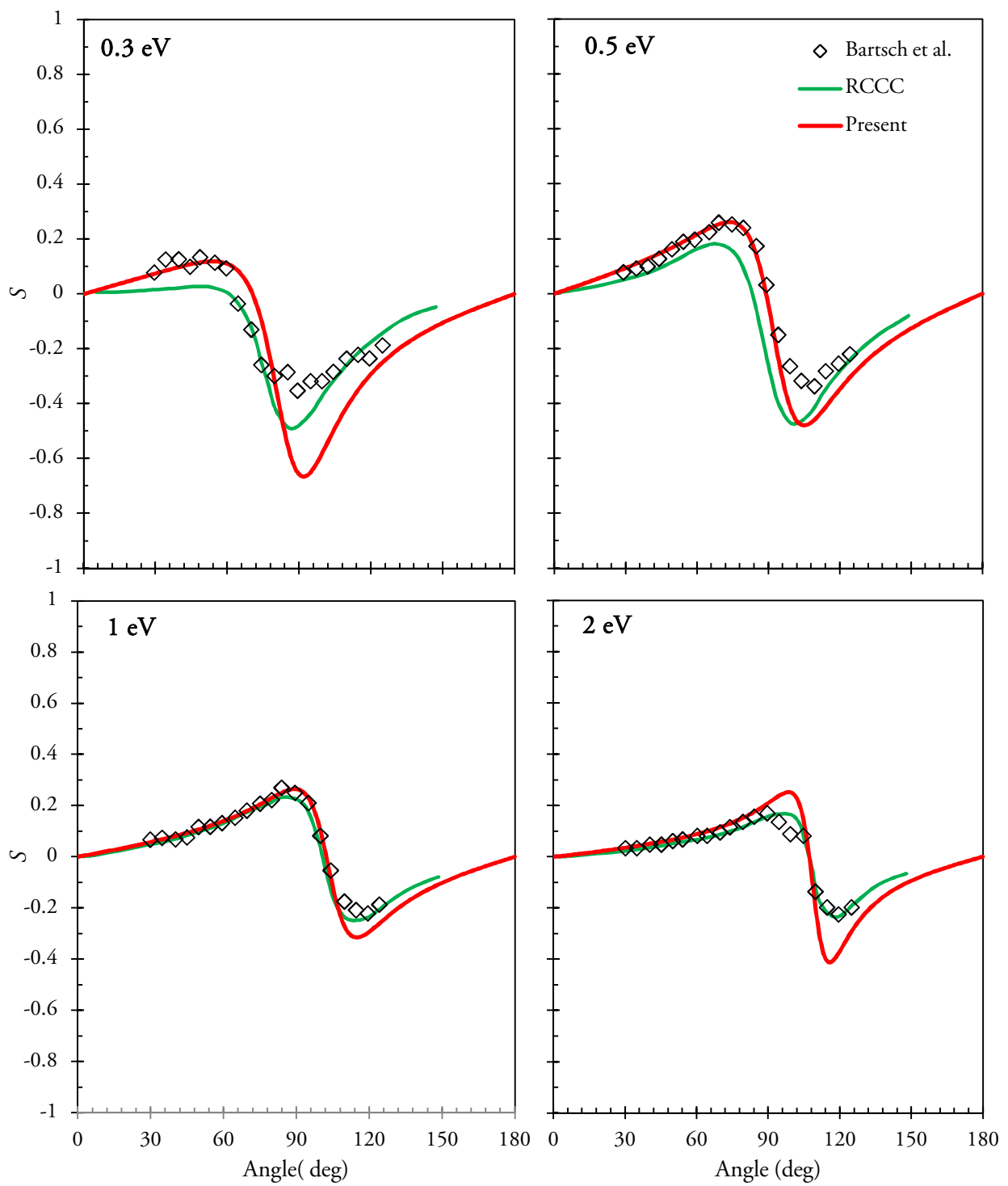


FIG. 5: Sherman function for electron scattering from cadmium at 0.3, 0.5, 1 and 2 eV: The legend in the figure describes markers for Present work; Experiment: Bartsch et al. [1]; Other theoretical: 55-state RCCC [7] calculations.

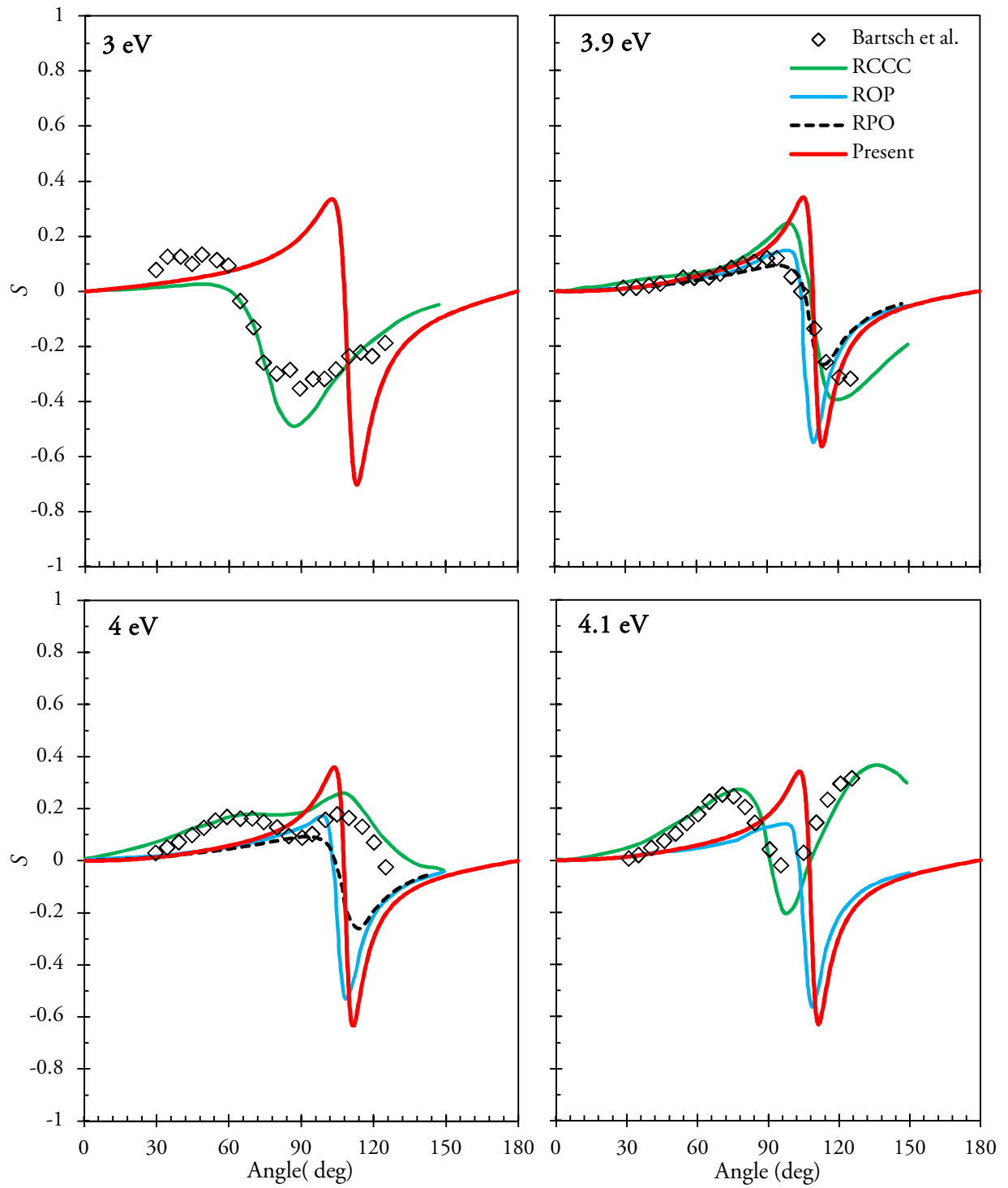


FIG. 6: Same as for figure 5 but at 3, 3.9, 4 and 4.1 eV projectile energies. Additional theoretical works are ROP [7] and RPO [4] calculations.

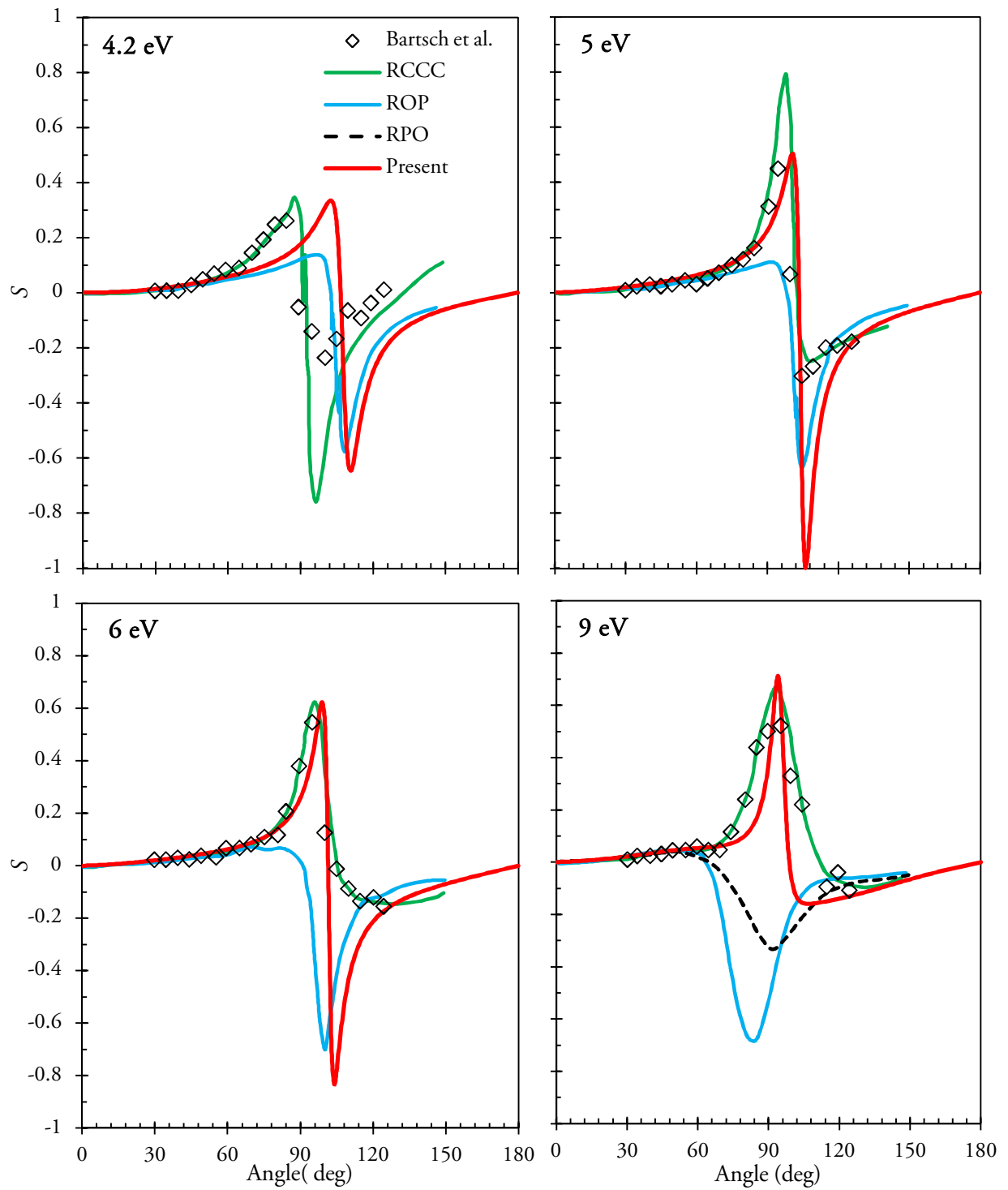


FIG. 7: Same as for figure 6 but at 4.2, 5, 6 and 9 eV projectile energies.

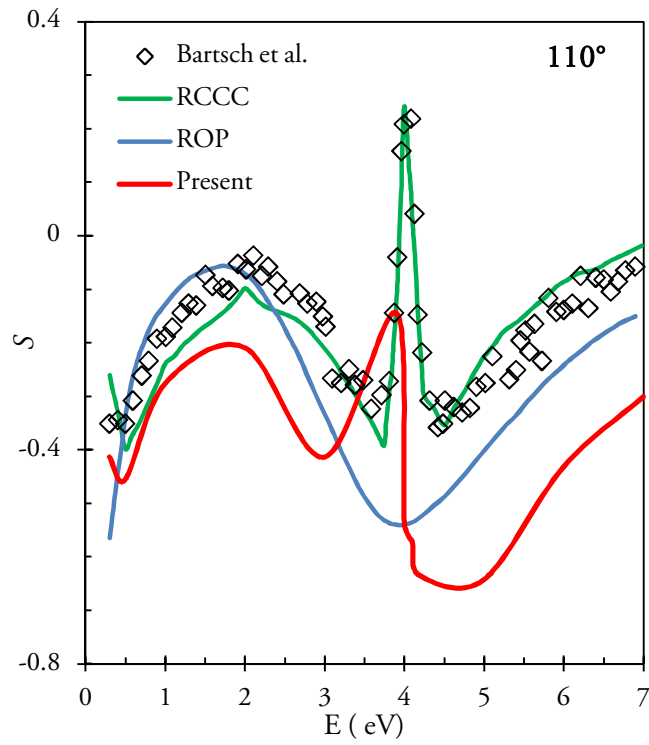


FIG. 8: Sherman function for electron scattering from cadmium at scattering angle  $110^\circ$  versus impact energy. The legend in the figure describes markers for Present work; Experiment: Bartsch et al. [1]; Other theoretical: 55-state RCCC [7] and ROP [7] calculations.

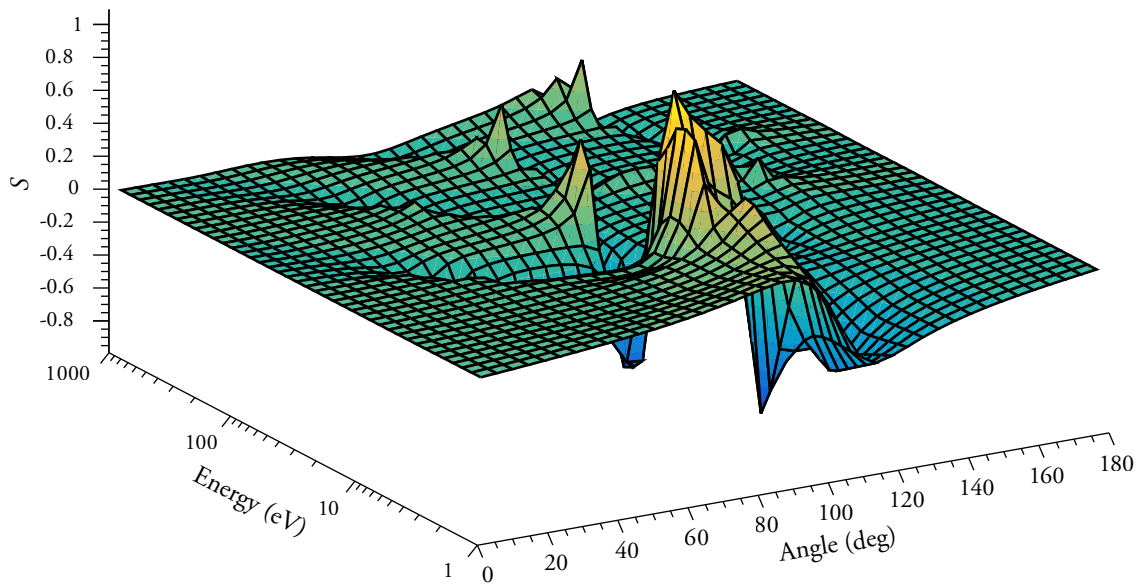


FIG. 9: A three-dimensional view of Sherman function for electron scattering from cadmium.

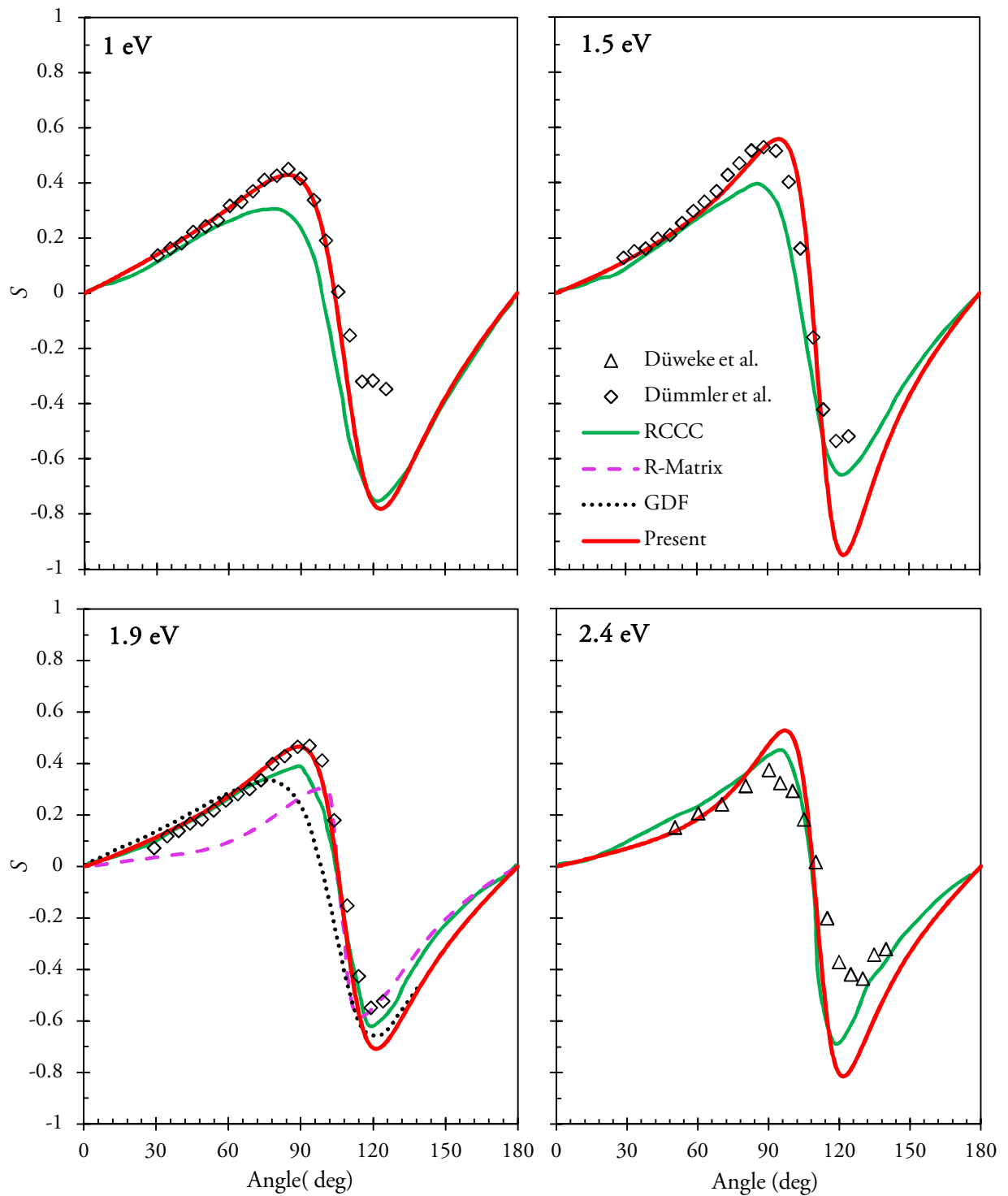


FIG. 10: Sherman function for electron scattering from mercury at 1, 1.5, 1.9 and 2.4 eV: The legend in the figure describes markers for Present work; Experiment: Düweke et al. [15] and Dümmler et al. [22]; Other theoretical: 66-state RCCC [5], R-matrix [26] and GDF [27].

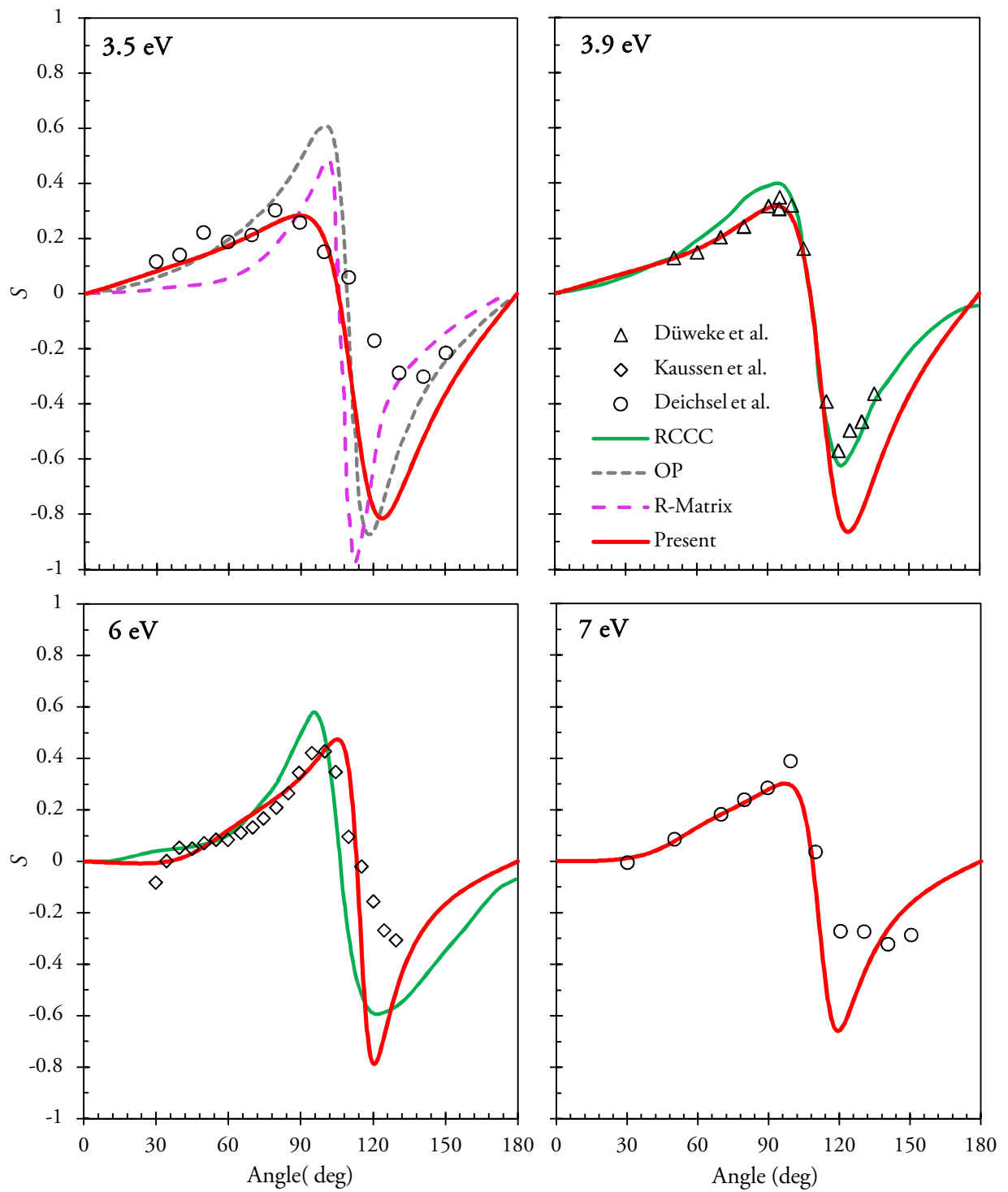


FIG. 11: Same as for figure 10 but at 3.5, 3.9, 6 and 7 eV projectile energies. Additional experiments: Kaussen et al. [21] and Deichsel et al. [11]; Additional theoretical: OP [32].

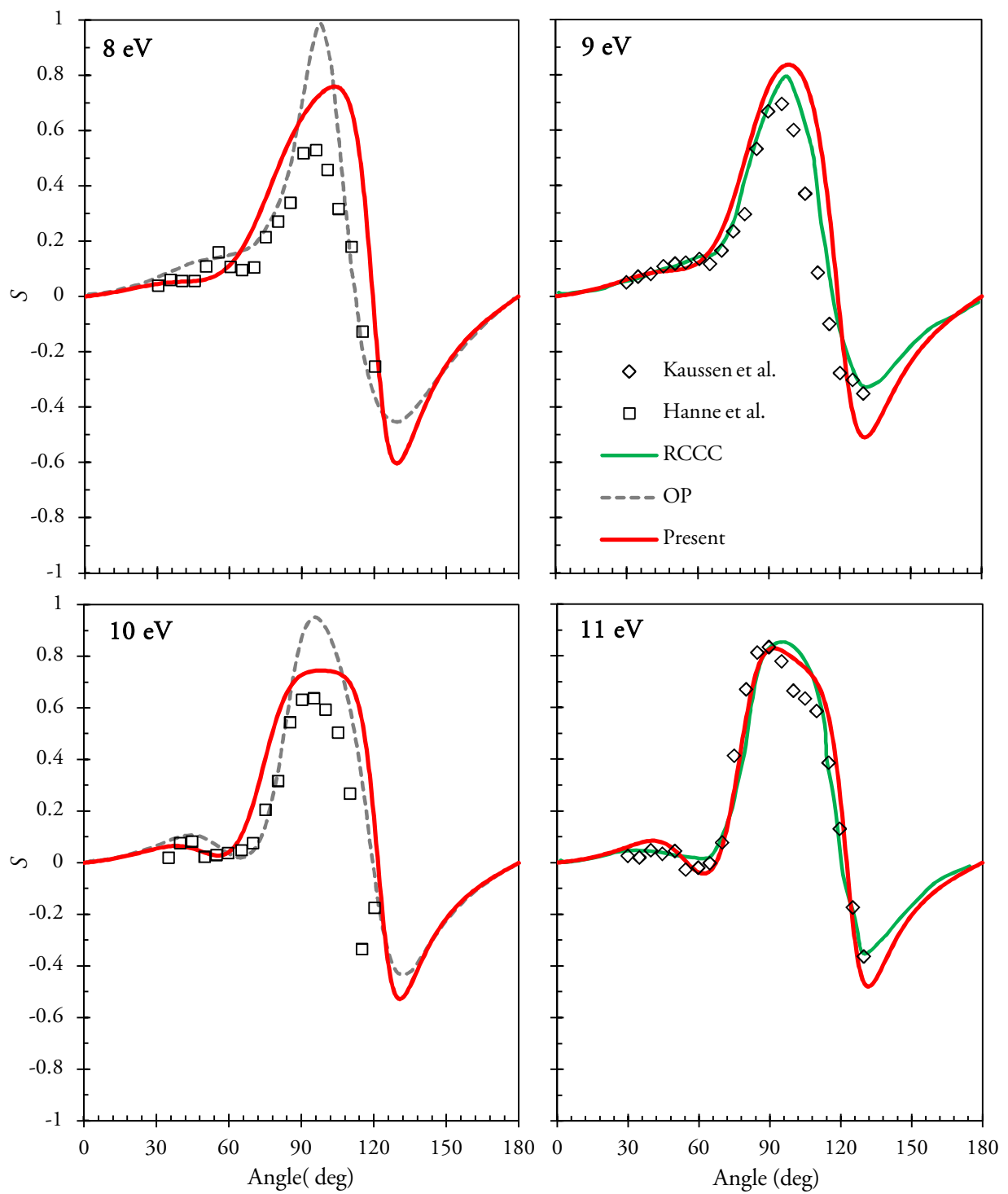


FIG. 12: Same as for figure 11 but at 8, 9, 10 and 11 eV projectile energies. Additional experiment is Hanne et al. [17].

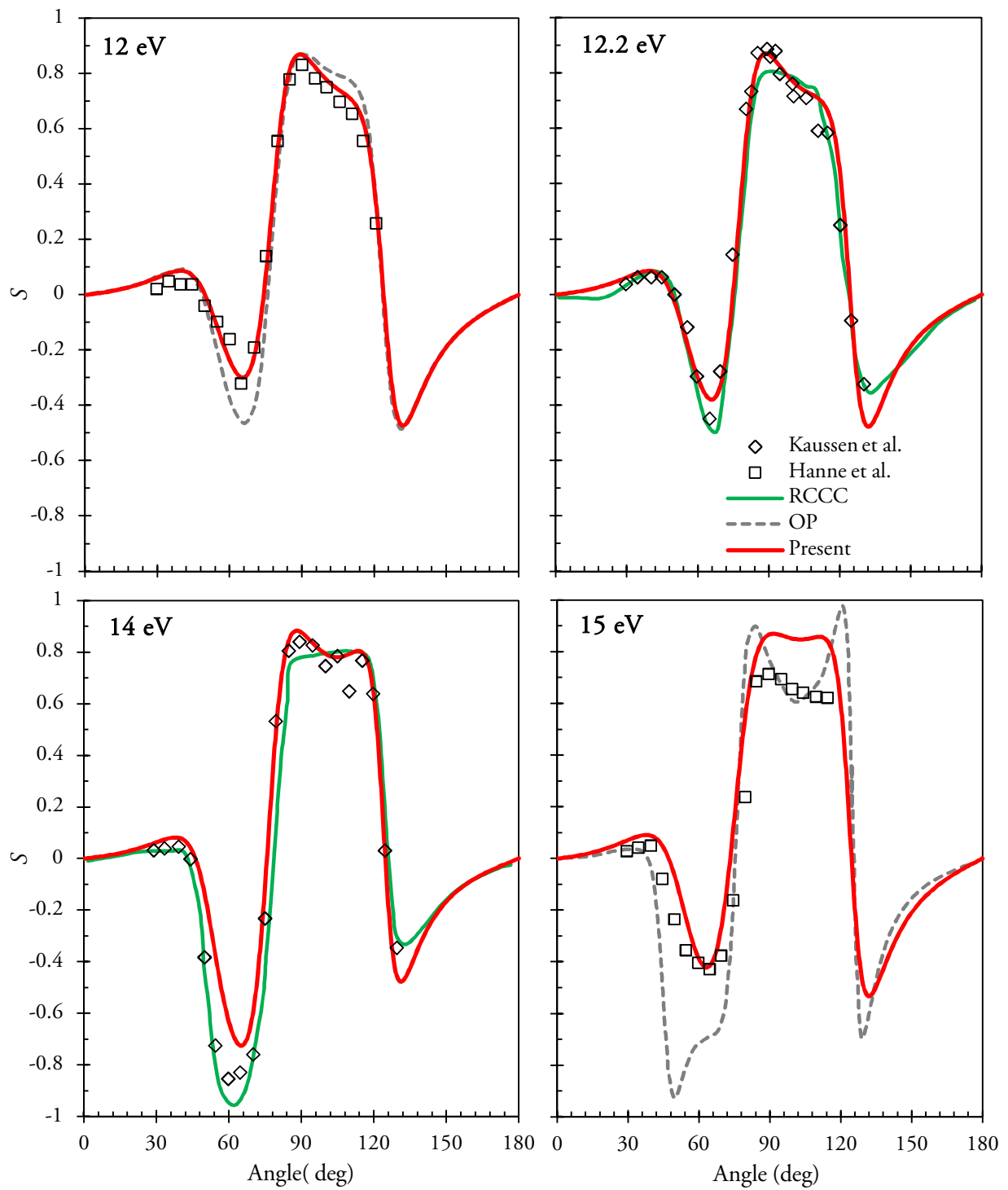


FIG. 13: Same as for figure 12 but at 12, 12.2, 14 and 15 eV projectile energies.

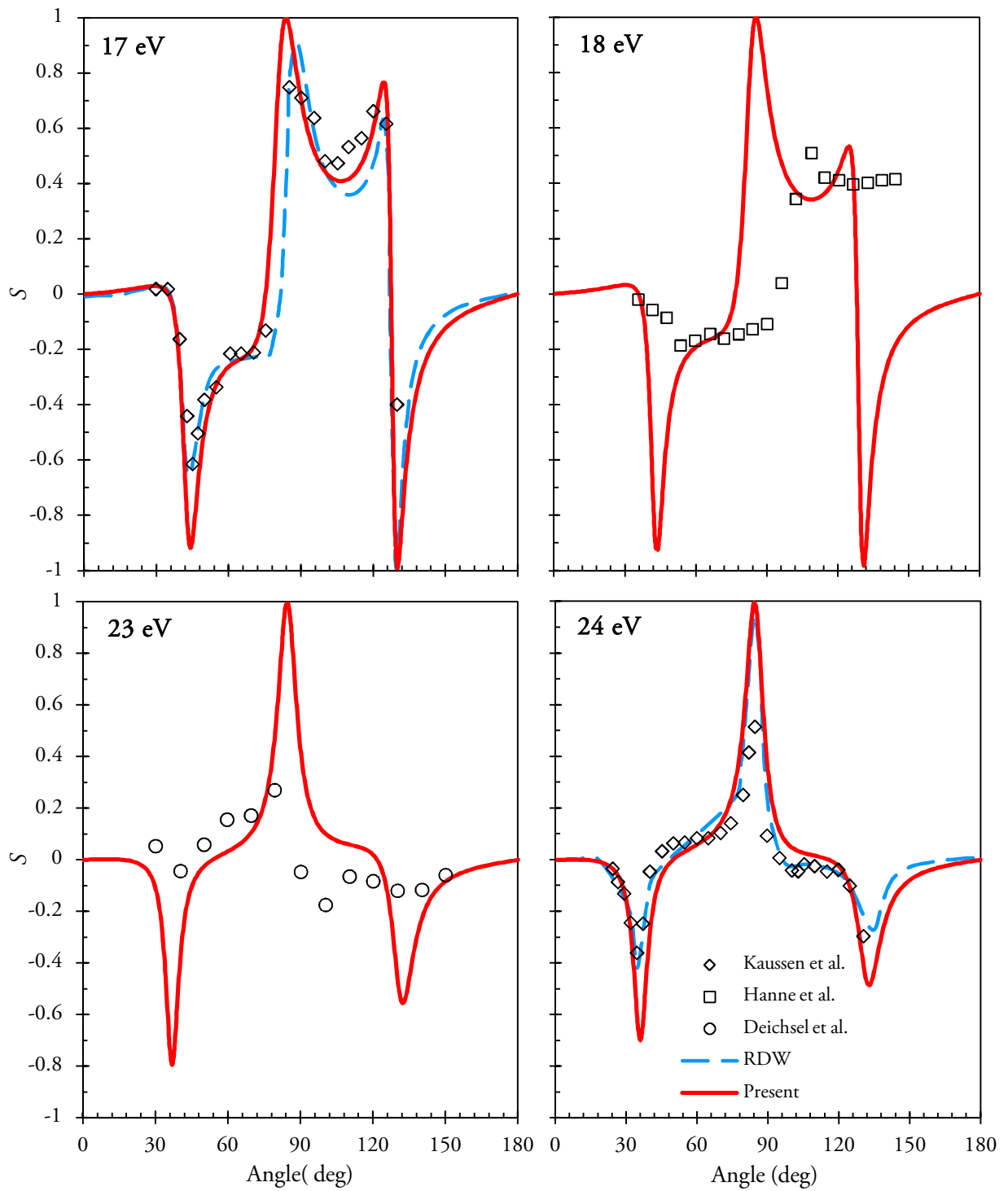


FIG. 14: Same as for figures 11 and 13 but at 17, 18, 23 and 24 eV projectile energies. Additional theoretical work is RDW [28].

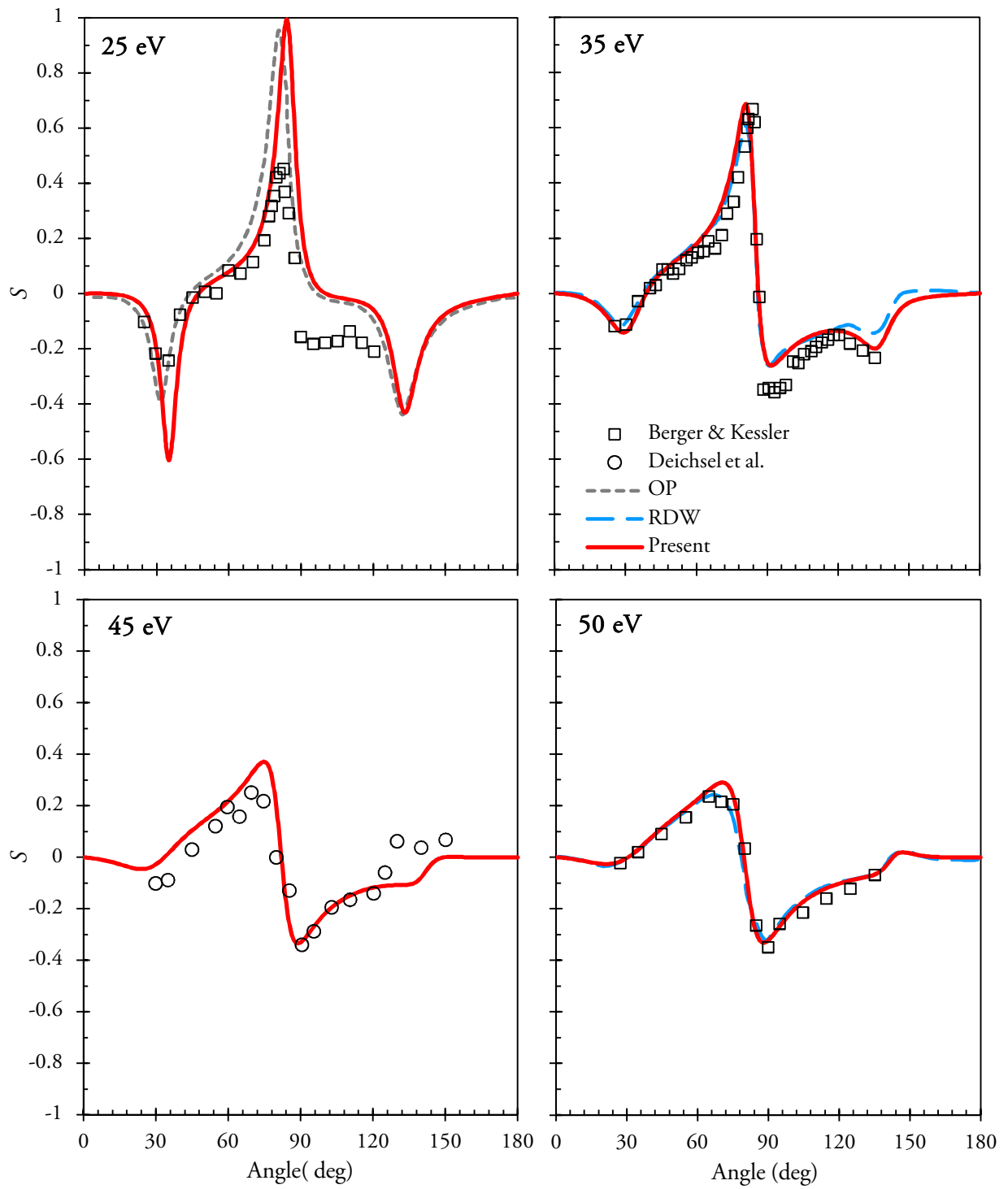


FIG. 15: Same as for figures 11 and 14 but at 25, 35, 45 and 50 eV projectile energies. Additional experiment is Berger and Kessler [20].

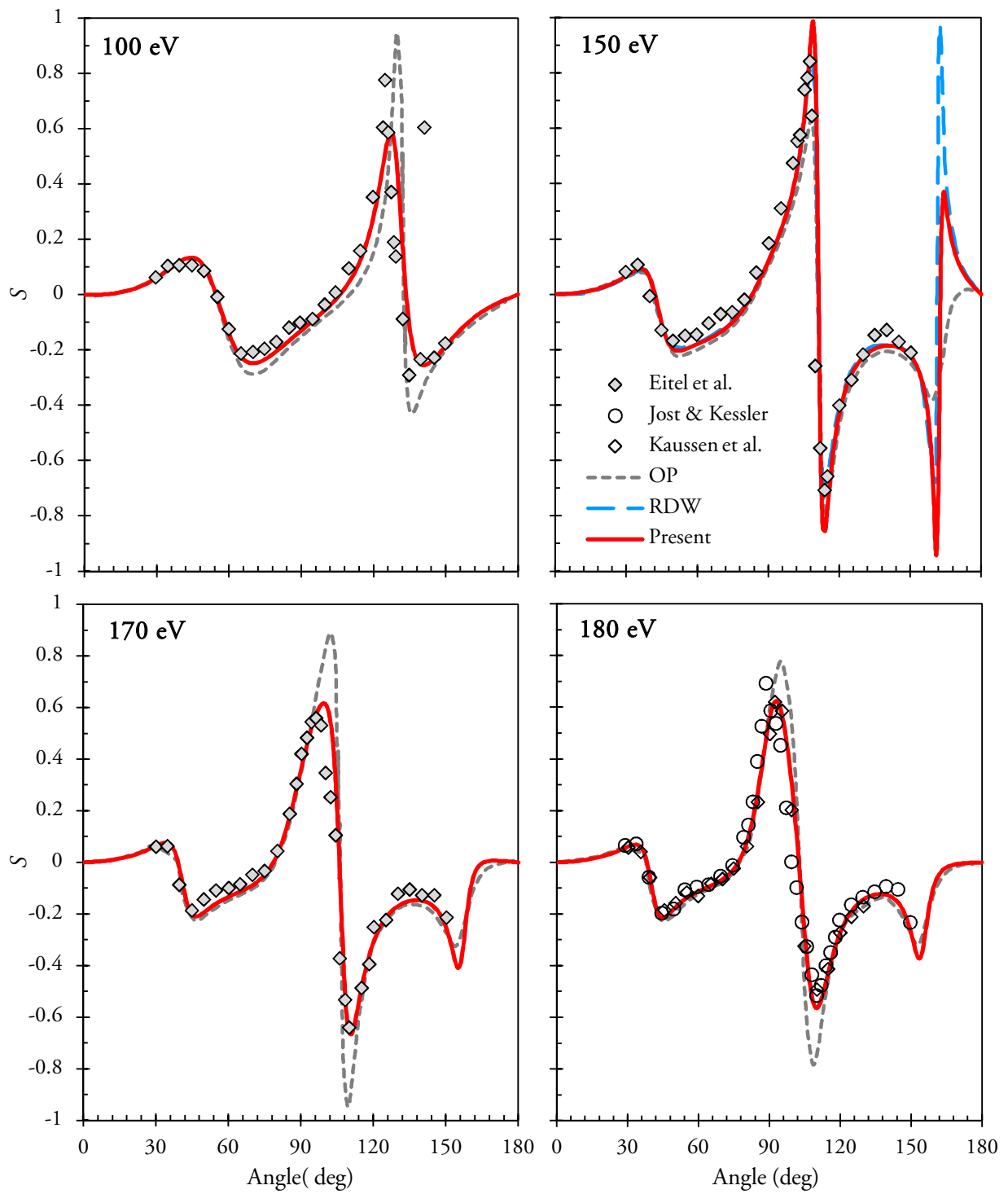


FIG. 16: Same as for figures 15 but at 100, 150, 170 and 180 eV projectile energies. Additional experiments are Jost and Kessler [10] and Eitel et al. [12].

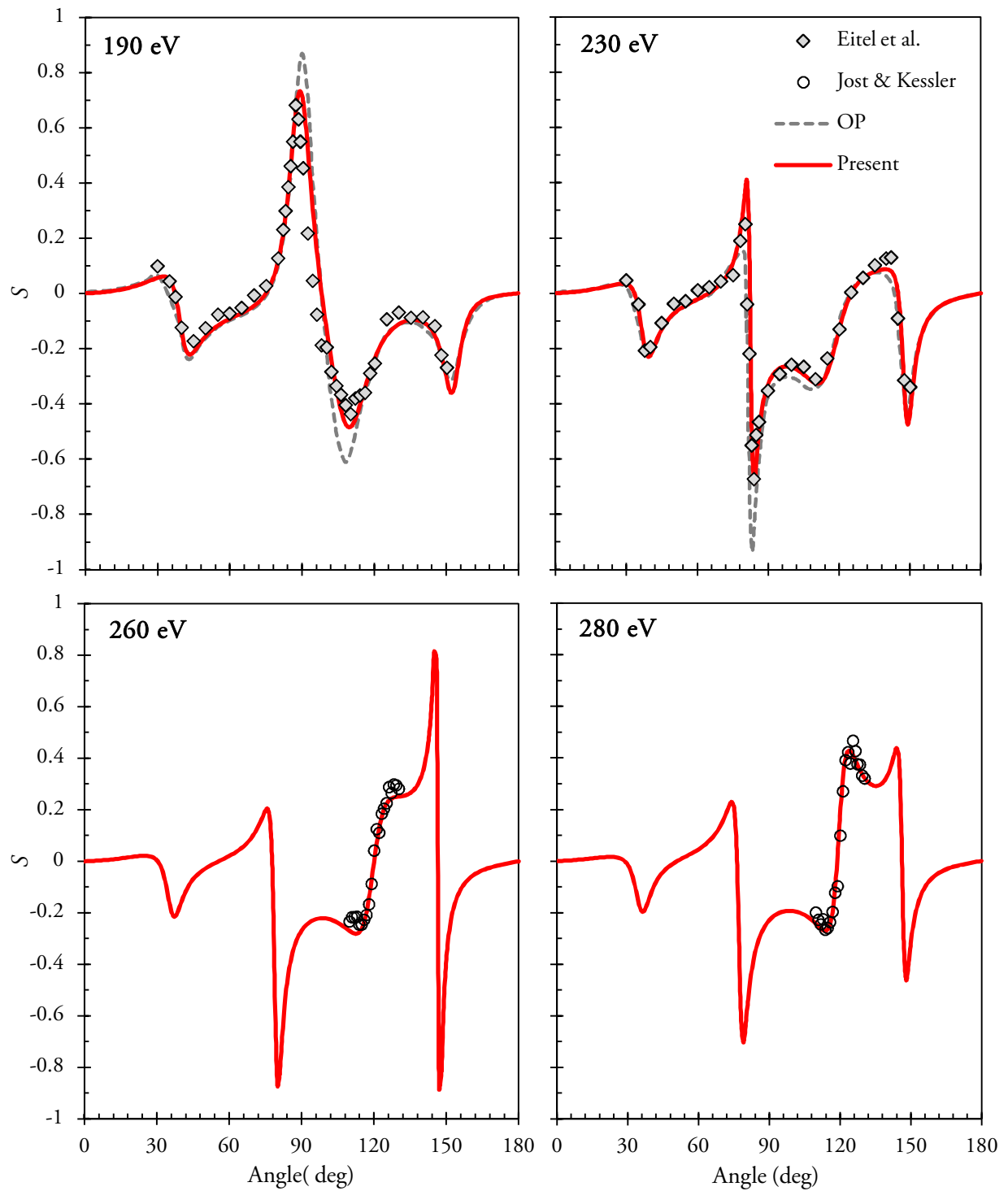


FIG. 17: Same as for figures 16 but at 190, 230, 260 and 280 eV projectile energies.

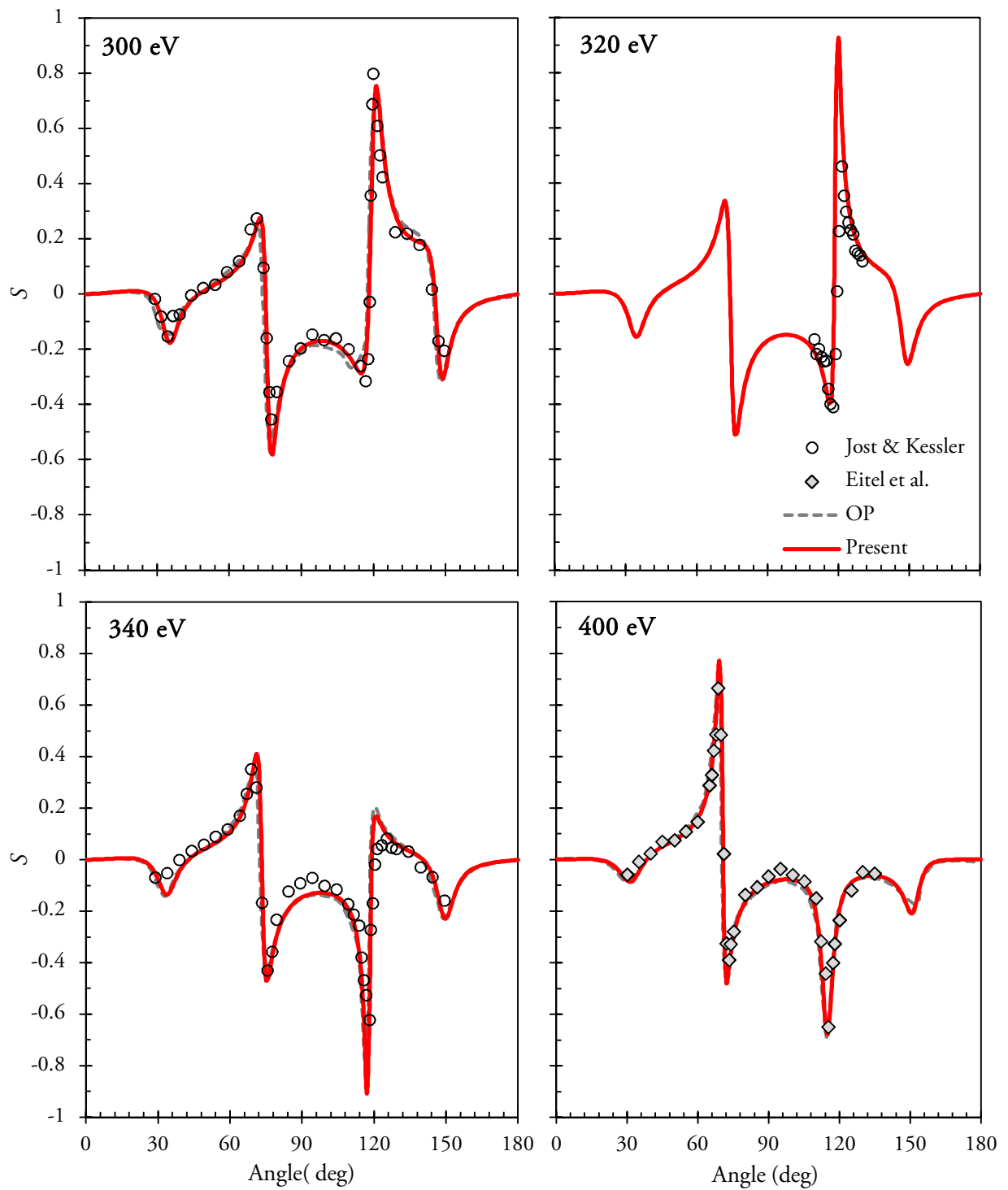


FIG. 18: Same as for figures 17 but at 300, 320, 340 and 400 eV projectile energies.

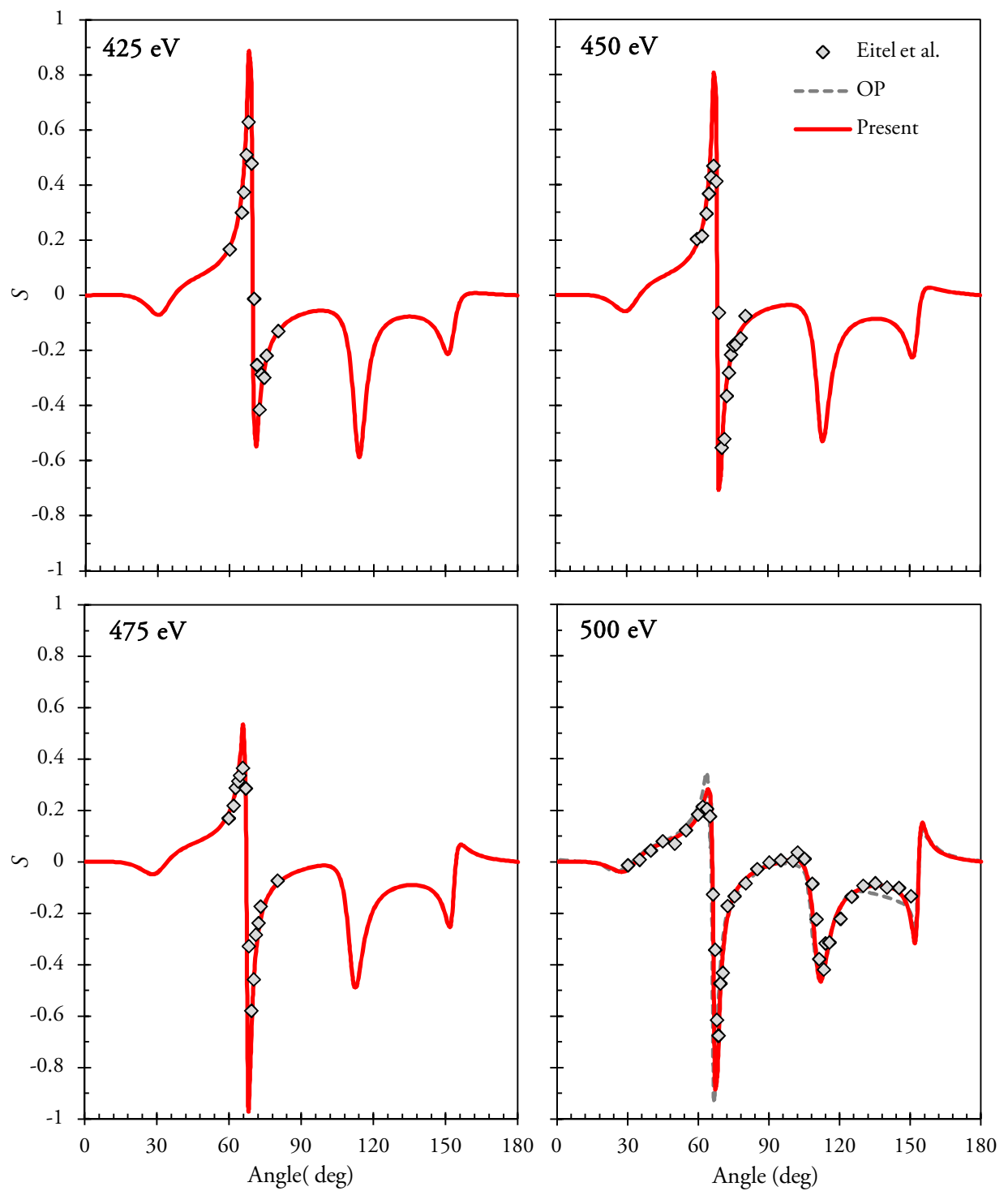


FIG. 19: Same as for figures 18 but at 425, 450, 475 and 500 eV projectile energies.

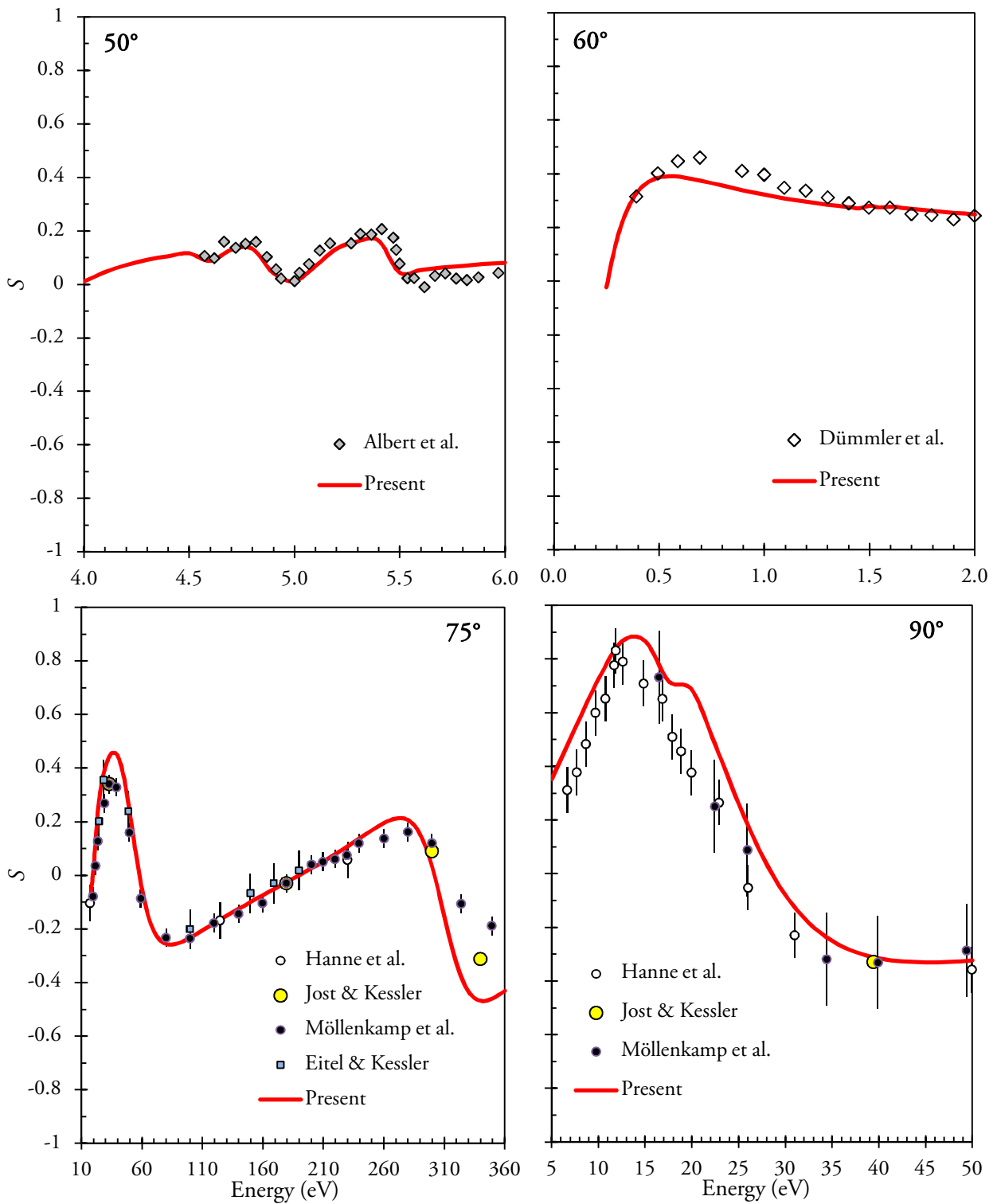


FIG. 20: Sherman function for electron scattering from mercury at 50°, 60°, 75° and 90° scattering angles. The legend in the figure describes markers for Present work; Experiment: Albert et al. [16], Dümmler et al. [22], Hanne et al. [17], Jost and Kessler [10], Möllenkamp et al. [19] and Eitel and Kessler [13]

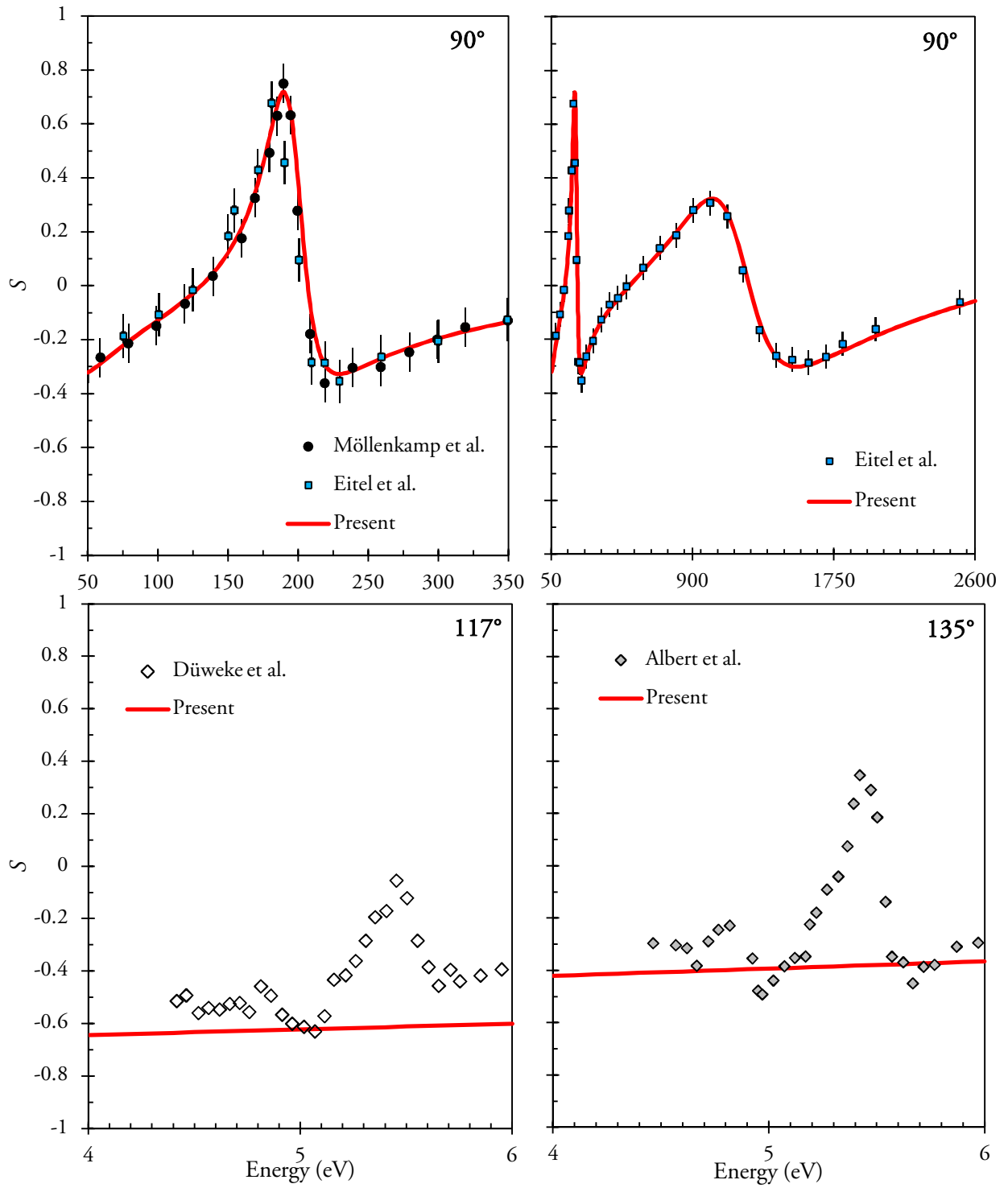


FIG. 21: Same as for figures 20 but at  $90^\circ$ ,  $117^\circ$  and  $135^\circ$  scattering angles. Additional experiment is Düweke et al. [15].

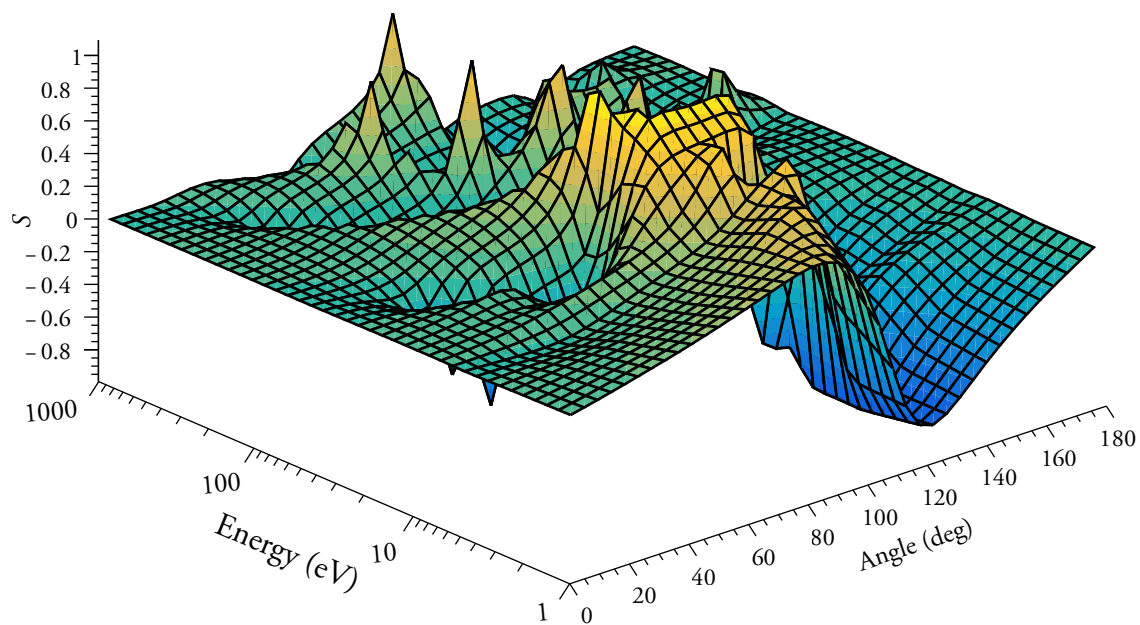


FIG. 22: A three-dimensional view of Sherman function for electron scattering from mercury.